J. Fluid Mech. (2007), *vol.* 581, *pp.* 69–78.
doi:10.1017/S0022112007005915 Printed in the United Kingdom

Axisymmetric liquid-metal pipe flow through a non-uniform magnetic field containing a neutral point

RICHARD G. KENNY

Department of Electronics, University of Hyogo, 2167 Himeji, Hyogo, 671-2201 Japan

(Received 13 October 2006 and in revised form 25 January 2007)

Axisymmetric liquid-metal pipe flow passes through a quadrupole magnetic field that is generated by a pair of 'oppositely sensed' d.c. current coils. As a result of this arrangement, the flow experiences a degree of braking, mostly in the vicinity of the magnetic neutral point, owing to the effect of Lorentz forces acting upon the liquid-metal. Usefully, the system represents a practical and novel electromagnetic (e.m.) valve capable of regulating the flow of molten metal emanating from a tun-dish, for example. Linear theory predicts the development of a counter-intuitive unidirectional 'slug-like' profile throughout the liquid-metal pipe flow at large values of the Hartmann number, M, in the presence of an idealized axisymmetric neutral point that extends to infinity. We confirm that this behaviour is also apparent, but over a narrow region spanning the neutral point, in the case of a more realistic liquid-metal pipe flow acted upon by a pair of oppositely sensed d.c. current coils. The axial pressure gradient along the wall of this flow manifests a sharp peak at large M centred on the neutral point that is generated by the steep gradients in the slug profile there. In fact, the pressure drop developed across this region is approximately equal to the net braking effect of the e.m. valve.

1. Introduction

A novel and practical d.c. electromagnetic (e.m.) valve can be formed from a pair of oppositely sensed d.c. current coils that are concentric to a given pipe or jet liquid-metal flow. The axisymmetric quadrupole magnetic field, or neutral point field, of the arrangement provides an effective means of non-invasively controlling the downspout flow of a liquid-metal from a tun-dish into a receptacle of solidifying melt, for example.

In this paper, we examine the nature of the e.m. braking effected by this d.c. field and, particularly, the dependence of the pressure drop at fixed mass flow rate (and vice versa) at large field strengths upon suitably defined Hartmann ($M \leqslant 100$) and Reynolds ($Re \leqslant 50$) numbers. A schematic of the idealized situation is presented in figure 1. Initially, a liquid-metal flow impinges upon a well-defined region of magnetic field and experiences some retardation there. Subsequently, downstream of the field region the flow recovers over a suitably long length of pipe to be a satisfactory approximation to Poiseuille flow. Although more pronounced effects upon the flow can be achieved with extended solenoids, as opposed to the two d.c. coils comprising our simplified e.m. valve, we anticipate that the liquid-metal flow will exhibit the same qualitative behaviour in both cases.

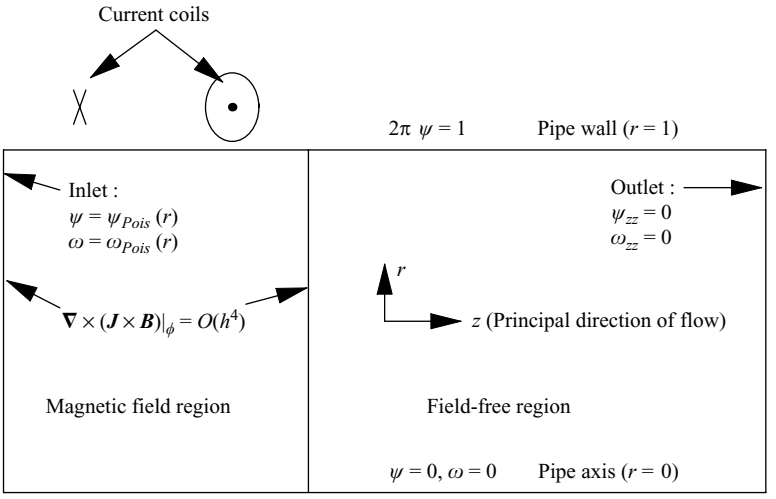

FIGURE 1. Axisymmetric liquid-metal flow in the upper half of an insulating pipe impinging upon a d.c. quadrupole magnetic field and, subsequently, recovering over a field-free region. Note that $\nabla \times (\boldsymbol{J} \times \boldsymbol{B})|_{\phi}$ is the azimuthal component of the curl of the Lorentz force and h is the grid spacing in the $O(h^4)$ finite-difference scheme.

In Kenny (1992), I considered the two-dimensional analogue to the proposed pipe flow of the current paper, namely, liquid-metal duct flow impinging upon a region of non-uniform magnetic field generated by four symmetrically arranged line currents. The corresponding numerical model for which yielded jet-like profiles at large Hartmann numbers, M, for the axial velocity component in the vicinity of the neutral point. This localized behaviour was consistent with the analytical results of linear theory that described unidirectional duct flow through an idealized neutral point extending to infinity. In that paper, and as part of a general consideration of magnetic fields that permit unidirectional flows to exist, it was seen that an idealized axisymmetric neutral point extending to infinity led to the development of a counter-intuitive 'slug-like' profile at large M throughout the flow. This was explained in terms of the 'curl' of the Lorentz force approximately vanishing over the core of such flows for asymptotically large M. We shall confirm that this aspect also applies to the more realistic case of flow in the vicinity of the axisymmetric neutral point of the arrangement shown in figure 1, by employing a highly accurate finite-difference algorithm with spacing h to model the associated streamfunction-vorticity equation.

2. Equations

The non-dimensional equations of steady incompressible liquid-metal magneto-hydrodynamic (MHD) flow can be written in the following manner:

$$\frac{1}{Re}\nabla^2 \boldsymbol{\Omega} - (\boldsymbol{u} \cdot \nabla)\boldsymbol{\Omega} + (\boldsymbol{\Omega} \cdot \nabla)\boldsymbol{u} = -N\nabla \times (\boldsymbol{J} \times \boldsymbol{B}), \tag{2.1}$$

$$\boldsymbol{J} = \boldsymbol{E} + \boldsymbol{u} \times \boldsymbol{B}, \quad \boldsymbol{B} = \boldsymbol{B}_0 + \boldsymbol{b}, \tag{2.2}$$

in which $\boldsymbol{\Omega} = \nabla \times \boldsymbol{u}$ is the vorticity vector, $\boldsymbol{B}$ is the total magnetic field and, where the electric field $\boldsymbol{E}$ and current density $\boldsymbol{J}$ obey the steady form of Maxwell's equations

namely,

$$\nabla \cdot \boldsymbol{J} = 0, \qquad \nabla \times \boldsymbol{E} = 0, \quad \nabla \times \boldsymbol{b} = R_m \boldsymbol{J}. \tag{2.3}$$

In the present context, the axial component of $\boldsymbol{E}$ vanishes along the wall of the non-conducting pipe in figure 1 so that $\boldsymbol{E} = 0$ everywhere by virtue of the assumption of axisymmetry and (2.3). The parameters related to (2.1)–(2.3) are the interaction parameter N, Hartmann number M, magnetic Reynolds number R_m, and Reynolds number Re, which are given by

$$N = \sigma B_N^2 a/(U_0 \rho), \quad M^2 = \sigma B_N^2 a^2/\mu, \quad R_m = a U_0 \sigma \mu_0, \quad Re = M^2/N. \tag{2.4}$$

Furthermore, in (2.4) and with reference to figure 1, a is the radius of the pipe, U_0 is a typical value of the axial component of flow and, B_N is the first-order approximation of the imposed field (non-dimensionalized to $\boldsymbol{B}_0$) in the vicinity of the neutral point. The liquid-metal is specified to have the following physical properties, namely, a permeability of μ_0, conductivity σ, density ρ and 'eddy viscosity' μ to account for any turbulence that might be present in the flow.

The type of metals considered in this study satisfy $R_m \ll 1$ (Shercliff 1965) which, in this limit, is approximately the ratio of the induced field $\boldsymbol{b}$ to a characteristic value of the imposed field $\boldsymbol{B}_0$ (cf. (2.2)). Consequently, to first order in R_m, we ignore the nonlinear interaction between the velocity and induced magnetic field and set $\boldsymbol{B} \approx \boldsymbol{B}_0$.

Equation (2.1) is linearized to yield unidirectional solutions when both the terms $(\boldsymbol{u} \cdot \nabla)\boldsymbol{\Omega}$ and $(\boldsymbol{\Omega} \cdot \nabla)\boldsymbol{u}$ vanish and the magnetic field is of a certain functional form (Kenny 1992). Examples of such solutions include the well-known Hartmann flow in the presence of a uniform transverse field in plane geometry and, less familiarly, the neutral point flow in both plane (Regirer 1960) and cylindrical geometries (Pai 1954).

The axisymmetry of figure 1 permits the introduction of a suitable streamfunction defined by $\boldsymbol{u} = (v, 0, u) = \nabla \times (\psi(r, z)\hat{\boldsymbol{\phi}}/r)$ so that we obtain a simplified scalar equation for the azimuthal component of the vorticity, $\omega(r, z)$, namely

$$\frac{1}{Re}\nabla^2\omega - (\boldsymbol{u} \cdot \nabla)\omega - \frac{\omega}{r^2 Re} + \frac{v(r, z)\omega}{r} = -N\left\{ r\left(\frac{\boldsymbol{B}_0 \cdot \nabla}{r}\right)^2 \psi - \left(\frac{\boldsymbol{B}_0 \cdot \nabla \psi}{r^2}\right)(\boldsymbol{B}_0 \cdot \hat{\boldsymbol{r}})\right\}, \tag{2.5}$$

where $\boldsymbol{\Omega} = (0, \omega(r, z), 0)$ and $\omega = -(1/r)(\nabla^2\psi - 2\psi_r/r)$. The numerical method employed to solve the coupled equations for ψ and ω is analogous to the approach used in Kenny (1992) and implements the 'compact explicit h^4 finite-difference approximations to operators of the Navier–Stokes type' summarized in Dennis & Hudson (1985).

3. Boundary conditions

In figure 1, we will assume Poiseuille conditions at both the entrance and exit of the 'field-free' regions of the pipe to enable a more convenient identification of the hydromagnetic component of the pressure drop over the length of the pipe to be made. Ultimately, it is this much larger component, with respect to any background hydrodynamic component, we wish to quantify in terms of known parameters that characterize the flow.

If required, somewhat higher values of Re can be accessed without recourse to prohibitively long pipes by relaxing the specification of Poiseuille conditions at the pipe exit and, instead, applying the weaker constraints $\omega_{zz} = 0$ and $\psi_{zz} = 0$ at the

outlet. The specification of ψ and ω on the boundary of the domain is complete when we impose both unit volume flux, i.e. $2\pi\psi = 1$, and no-slip conditions at the wall ($r = 1$) in addition to symmetry requirements along the axis of the pipe, cf. figure 1.

The axial extent of the field region is determined from where the Lorentz forcing term, $\nabla \times (\boldsymbol{J} \times \boldsymbol{B}_0)$, in (2.5) is equal to the $O(h^4)$ error estimate in the corresponding numerical algorithm. Consequently, a smooth transition to the downstream 'field free' region is anticipated over which hydrodynamic recovery to a good approximation of Poiseuille flow is possible. An estimation of this recovery length can be made using vorticity diffusion arguments as discussed in Kenny (1992).

4. Quadrupole magnetic field

It is convenient to employ a scalar streamfunction χ with which to express a vacuum field $\boldsymbol{B}_0'$ generated by an axisymmetric distribution of current, so that $\boldsymbol{B}_0' = \nabla \times (\chi \hat{\boldsymbol{\phi}}/r)$. As a result, the streamfunction χ of a current coil centred at the origin of coordinates and suitable for rapid numerical evaluation is given by

$$\chi(r, z) = \frac{\mu_0 I}{2\pi} \sqrt{z^2 + (r+\gamma)^2} \left[-E(m) + \frac{z^2 + r^2 + \gamma^2}{z^2 + (r+\gamma)^2} K(m) \right], \tag{4.1}$$

where $r = 1$ corresponds to the pipe wall, γ is the ratio of the coil to pipe radius a, I is the coil current, $m = 4r\gamma/(z^2 + (r+\gamma)^2)$ and, $K(m)$ and $E(m)$ are complete elliptic integrals of the first and second kind, respectively (Abramovich & Stegun 1965, p. 591).

The quadrupole field in figure 1 can now be derived from (4.1) using coils located at $z = \pm z_0$. Generally, we set $z_0 = 1$ and $\gamma = 3/2$, but extend z_0 in cases where increased flow resolution in the inter-coil region is required. Near to the neutral point at the origin of coordinates, the scaling B_N in (2.4) is given by $B_N = 3\mu_0 I z_0 \gamma^2 / 2(z_0^2 + \gamma^2)^{5/2}$.

5. Results

5.1. *Comparison of numerical and analytical profiles*

The analytical result for unidirectional flow in a neutral point field extending to infinity was originally derived by Pai (1954), and which for our purposes can be expressed as

$$u(r) = (M/\pi) \left[\cosh(M/2) - 1\right]^{-1} \int_{M^{1/2} r}^{M^{1/2}} \sinh(\xi^2/2)/\xi \, \mathrm{d}\xi. \tag{5.1}$$

The numerical solution of (2.5) at the neutral point $z = 0$ is unidirectional to a high degree of accuracy and compares well with the relatively flat form of (5.1) for $M = 10$ and $Re = 1$ (figure 2). The extent of the profile flattening can be estimated in the asymptotic limit of large M when the condition of unit flux implies that $\lim_{M \to \infty} u(r) \sim 1/\pi \sim 0.32$, ignoring the contribution from the Hartmann boundary layer at the wall ($r = 1$).

5.2. *Evolution of pipe flow*

Figure 3 records various profiles for the case of $M = 10$ ($z_0 = 3$, $Re = 1$), where it is recalled that the current coils are located at $\pm z_0$. For clarity, only the most significant features of flow evolution are depicted which occur over a relatively narrow range of pipe spanning the inter-coil region. Significantly, a slug profile is clearly apparent at the neutral point ($z = 0$) of the pipe flow.

In figure 4, the axial variation of the vorticity along the pipe suggests that discernible Hartmann boundary layers at the wall are only apparent for a narrow range centred

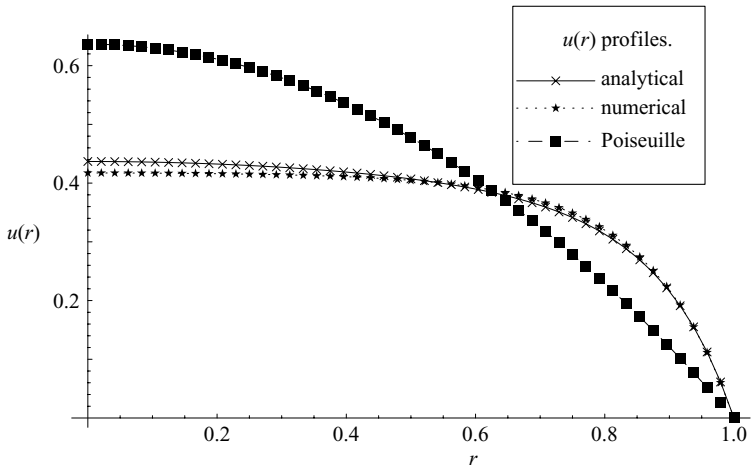

FIGURE 2. Comparison of numerical and analytical axial velocity profiles $u(r)$ at the neutral point $z=0$, for $M=10$ and $Re=1$. The Poiseuille velocity profile for unit volume flux in a pipe is included for reference.

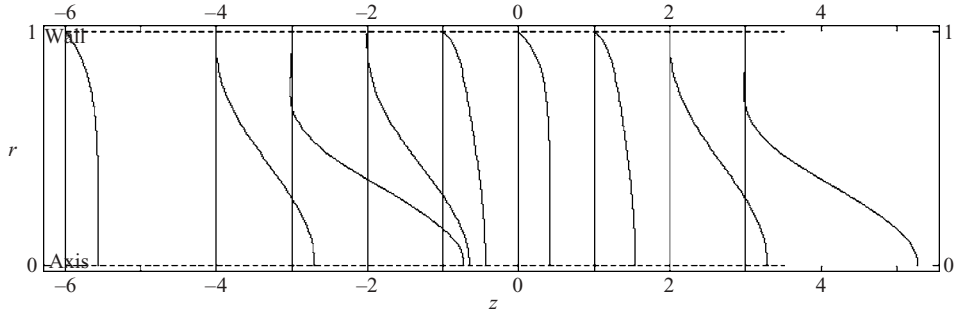

FIGURE 3. Evolution of u profiles along the pipe for $M=10$, $Re=1$ and $z_0=3$. For reference, at the wall ($r=1$) $u=0$, $z=0$ denotes the neutral point, $z=\pm 33$ corresponds to the edges of the magnetic region, and $z=35$ is the location of the pipe exit.

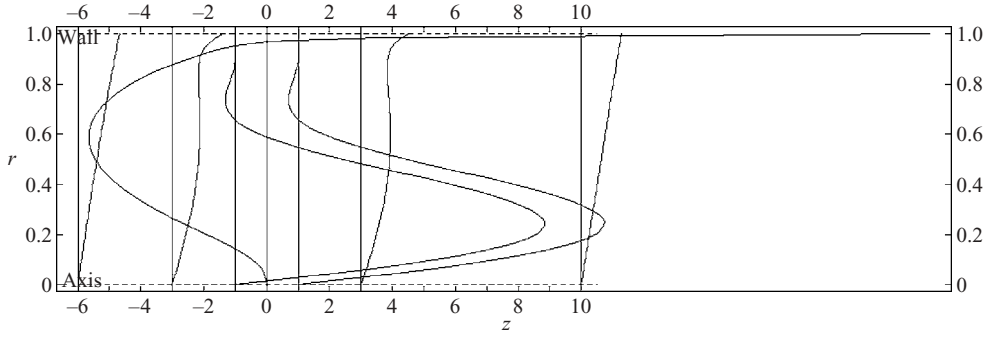

FIGURE 4. Evolution of ω profiles along the pipe for $M=100$, $Re=1$ and $z_0=1$.

on the neutral point. In the next section, scaling arguments for asymptotically large M suggest that this axial length scale along the wall is $O(M^{-1/2})$. Although the same scale of variation exists in comparable duct flow, by contrast, no central jet structure

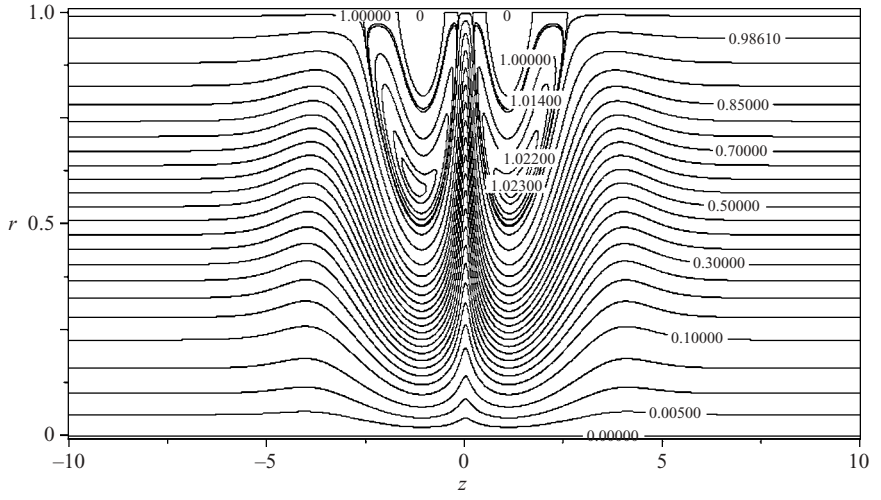

FIGURE 5. Scaled streamfunction contours, i.e. $2\pi\psi$, for $M = 100$, $Re = 1$ and $z_0 = 1$. Amplified stagnant flow regions exist beneath the current coils located at $z = \pm z_0$.

$N = M^2/Re$	Interaction parameter, or Stuart number cf. (2.4)
$\Delta P = \int_{z_1}^{z_2} \nabla^2 u/Re \, \mathrm{d}z$	Total pressure drop
$\Delta P_e = \Delta P - \int_{z_1}^{z_2} \nabla^2 u_{Pois}/Re \, \mathrm{d}z$	'Excess' pressure drop, cf. (5.2)
$\delta = O(M^{-1})$	Hartmann (radial) boundary layer width at $r \sim 1$
$\Delta z = O(M^{-1/2})$	Width of axial pressure gradient about $z = 0$ for $r \sim 1$

TABLE 1. Summary of terms and limiting length scales for $M \to \infty$ that appear in § 5.

emerges for the axisymmetric flow in this region, despite analogous tapering of the magnetic field lines. This is explained by the differing effects that the dominant core approximation of (2.1) at large M, i.e. $M^2\nabla \times (\boldsymbol{J} \times \boldsymbol{B}_0) \sim 0$, yields in axisymmetric and duct geometries (Regirer 1960; Kenny 1992).

Pronounced regions of stagnant flow are present beneath the current coils, as is evidenced by the streamfunction contour plot in figure 5 for $M = 100$ and $Re = 1$. These possibly represent an undesirable feature of the e.m. valve owing to the likelihood of a buildup in particulate or gaseous impurities that can impair metal quality.

5.3. *Fixed volume flux results*

In order to focus upon the contribution to the total pressure drop from the effect of the Lorentz forces acting upon the liquid-metal we define

$$\Delta P_e = \Delta P - (1/Re) \int_{z_1}^{z_2} \nabla^2 u_{Pois} \, \mathrm{d}z, \tag{5.2}$$

for a pipe of length $z_2 - z_1$, so that ΔP_e is the 'excess' pressure drop over and above that derived from the Poiseuille component of flow, see table 1. At large values of M, the excess pressure gradient at the wall $\partial P_e/\partial z|_{r=1}$ exhibits a sharp peak centred on the neutral point, as is suggested by figure 6. The corresponding pressure drop across

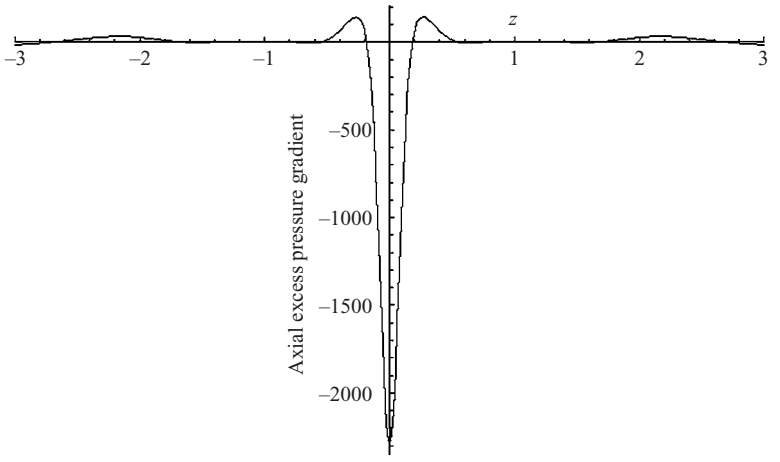

FIGURE 6. A plot of $\partial P_e/\partial z$ at $r = 1 - 2h$, in which $h \sim 1/75$ is the grid-spacing (for $Q = 1$, $M = 100$ and $Re = 1$), P_e against axial distance z spanning the inter-coil region. The current coils are located at $z = \pm 1$.

this narrow locality accounts for almost all the magnetic braking along the pipe. On this basis, the asymptotic behaviour of $Re\Delta P_e$ at large M can be estimated from the gradients across the Hartmann (radial) boundary layer of width δ namely,

$$\lim_{M\to\infty} Re\Delta P_e = \lim_{M\to\infty} \int_{z_1}^{z_2} \nabla^2(u - u_{Pois})\Big|_{r=1} \mathrm{d}z \sim \tilde{u}\Delta z/\delta^2 \sim QM^2\Delta z, \tag{5.3}$$

where $\delta = O(M^{-1})$, and $Q = \pi\tilde{u}$ is the volume flux from a slug flow with uniform core velocity $\tilde{u}$. The axial length scale Δz can be determined from the rapid vorticity variation about the neutral point, a feature that is clear from figure 4. At large M and $r \sim 1$, the next highest order of magnitude terms in the streamfunction–vorticity equation (2.5) satisfy

$$\omega_{zz} + \omega_r \sim -2M^2\Delta z\,\psi_{rz}, \tag{5.4}$$

which represents the balance between the viscous terms on the left-hand side and the e.m. forcing term on the right-hand side. For convenience, we simply balance the scaling of the terms on the left-hand side of (5.4) to yield

$$\Delta z^2 \sim \delta \quad \text{or} \quad \Delta z \sim M^{-1/2}. \tag{5.5}$$

Consequently, we may rewrite (5.3) as

$$\lim_{M\to\infty} Re\Delta P_e \sim QM^{3/2}, \tag{5.6}$$

which appears to be confirmed by figure 7 which compares a plot of the $(3/2)\log M$ asymptote with the quantity $\log(Re\Delta P_e)$. For clarity, a representative value of Re is specified to avoid blurring of the data.

As kindly suggested by one referee, it is instructive to compare (5.6) with an estimate of the excess pressure drop when the magnetic field is entirely transverse to the pipe flow (cf. Hua & Walker 1989). In this case, the core axial velocity profile is approximately hemispherical (Roberts 1967*b*, page 184), and scaling arguments in the limit of large M for this region yield

$$\lim_{M_T\to\infty} Re\Delta P_e \sim QM_T^2, \tag{5.7}$$

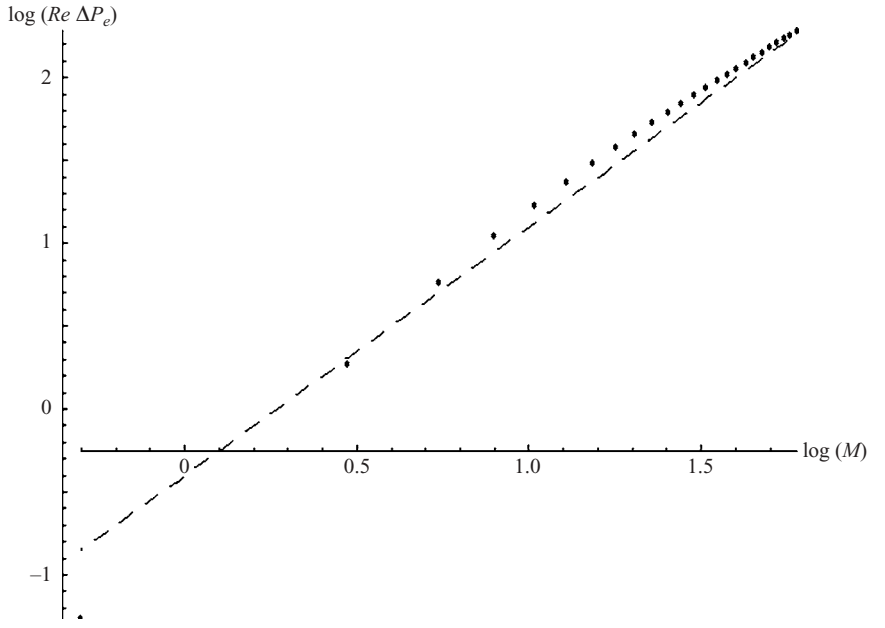

FIGURE 7. A plot of $\log(Re\,\Delta P_e)$ versus $\log(M)$ for unit flux, $Q=1$. For clarity, a specific value of Re is chosen, $Re=23$, to avoid data blurring. – – –, the logarithmic asymptote $(3/2)\log M$ in (5.6).

where M_T is a suitably defined Hartmann number for this flow. The relations (5.6) and (5.7) suggest that somewhat less electrical power is consumed by implementing a transverse field in place of a neutral-point configuration to enforce a specified pressure drop ΔP_e on a flow with a given Q/Re. Despite this advantage, however, the transverse field flow is characterized by the development of two high-velocity narrow sidewall jets (Roberts 1967*a*, *b*), which span regions where the field is approximately tangential to the wall. Residual jet structures are likely to still exist at the exit of a downspout to a tun-dish, for example, so that the depth to which any impurities and instabilities penetrate the solidifying melt below is increased in this case to yield impaired metal quality.

5.4. *Fixed pressure drop results*

Liquid-metal falling from a tun dish at a speed of $\sim 1\,\mathrm{m\,s^{-1}}$ tends to operate under the constraint of a fixed head of metal in an industrial context. Fortunately, and unlike other numerical schemes that divide the flow into core and boundary-layer regions (e.g. Hua & Walker 1989; Molokov & Reed 2003), advantage can be taken of a similarity relationship to generate data at a fixed pressure drop ΔP_e using data obtained at a fixed volume flux Q. This approach follows Kenny (1992) in which it was noted that similar flows result when ψ is scaled by α, Re by $1/\alpha$ and the pressure drop by a factor α^2 to yield

$$\Delta P_e(M, Re, Q) = (1/\alpha^2)\Delta P_e(M, Re/\alpha, \alpha Q). \tag{5.8}$$

Employing (5.8), it is now possible to invert the data more conveniently obtained at fixed Q to that at a set value of ΔP_e.

A plot of Q against N is given in figure 8 for various narrow bands of Re that result from the nature of the inversion process in (5.8). The effect of the magnetic braking is particularly apparent at low to moderate values of N. At large N in figure 8, it

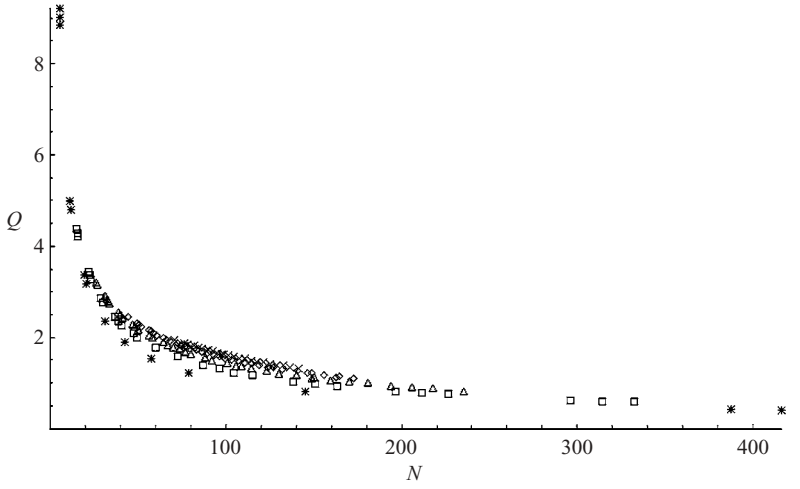

FIGURE 8. A plot of Q against N at fixed ΔP_e ($=-10.15$ units) for various narrow bands of Re values. Specifically, the bands of Re are $\pm 5\%$ of the following:
$*$, $Re = 5.345$; $\square$, $Re = 10.67$; $\triangle$, $Re = 15.99$; $\diamond$, $Re = 21.31$; $\times$, $Re = 26.63$.

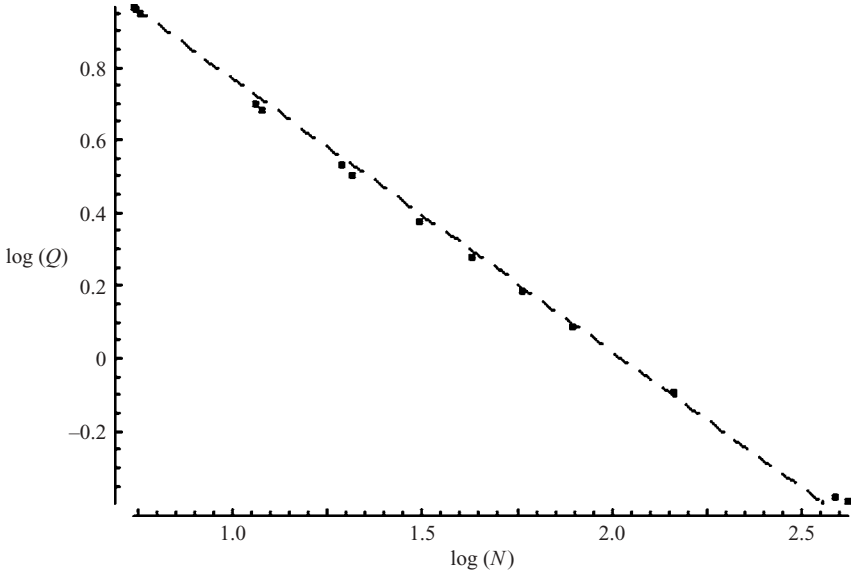

FIGURE 9. A plot of $\log Q$ against $\log N$ for $Re = 5.35$ and $\Delta P_e = -10.15$ units.
– – –, the logarithmic asymptote $(-3/4)\log N$ in (5.9).

appears that Q decreases asymptotically which suggests that the e.m. valve effectively brakes the metal flow to a small seepage.

The asymptotic behaviour of Q in the limit of large N at constant pressure drop can be derived from (5.6) to yield

$$\lim_{N\to\infty} Q \sim N^{-3/4} Re^{1/4} \Delta P_e, \tag{5.9}$$

the logarithm of which appears to agree closely with the corresponding data plotted in figure 9.

6. Conclusion

In this paper, we have shown that accurate numerical simulations for an axisymmetric liquid-metal pipe flow passing through a quadrupole field generated by two d.c. current coils becomes unidirectional in the vicinity of the neutral point. The associated flow profile is that of a 'slug type' and agrees well with the corresponding linear theory of unidirectional flow in an infinitely extended axisymmetric neutral point developed in Pai (1954) and Kenny (1992). Asymptotic arguments indicate that the axial length scale along the wall over which the pipe flow becomes unidirectional is $O(M^{-1/2})$. The corresponding axial pressure gradient exhibits a peak over this length scale that is interpreted as a sharp brake acting on the flow. Moreover, the retardation developed in this region accounts for almost all the pressure drop across the ends of the pipe and scales as $O(M^{3/2})$ which is confirmed by the numerical data generated at a fixed volume flux.

One major issue that remains to be addressed for a possible future study is the role of turbulence in the neutral point field of figure 1. Generally, magnetic fields dampen turbulent transverse flows but, possibly, enhance parallel velocity fluctuations (Lee & Choi 2001). The presence of significant axial components of field parallel to the principal direction of flow in figure 1 suggests that some component of turbulence should be accounted for. The degree to which it should be included though will depend critically upon the operational regime of M and Re.

The author is very grateful to both Professor Keith Moffatt (Department of Applied Mathematics and Theoretical Physics, University of Cambridge) and Dr A. J. Mestel (Department of Mathematics, Imperial College) for taking the time to both read and offer advice on the manuscript.

REFERENCES

Abramovich, M. & Stegun, I. A. 1965 *Handbook of Mathematical Functions*, 3rd edn. Dover.

Dennis, S. C. R. & Hudson, J. D. 1985 Compact explicit finite difference approximations to the Navier–Stokes equation. In *Ninth Intl Conf. on Numerical Methods in Fluid Dynamics* (ed. Soubbaramayer & J. P. Boujot), Lecture Notes in Physics, vol. 218, pp. 23–51. Springer.

Hua, T. Q. & Walker, J. S. 1989 Three-dimensional MHD flow in insulating circular ducts in non-uniform transverse magnetic fields. *Intl J. Engng Sci.* **27**, 1079–1091.

Kenny, R. G. 1992 Liquid-metal flows near a magnetic neutral point. *J. Fluid Mech.* **244**, 201–224.

Lee, D. & Choi, H. 2001 MHD turbulent flow in a channel at low magnetic Reynolds number. *J. Fluid Mech.* **439**, 367–394.

Molokov, S. & Reed, C. B. 2003 Parametric study of the liquid metal flow in a straight insulated circular duct in a strong nonuniform magnetic field. *Fusion Sci. Technol.* **32**, 200–216.

Pai, S. 1954 Laminar flow of an electrically conducting incompressible fluid in a circular pipe. *Appl. Phys.* **25**, 1205–1207.

Regirer, S. 1960 On an exact solution of the equations of magnetohydrodynamics. *Z. angew. Math. Mech.* **24**, 556.

Roberts, P. 1967*a* Singularities of Hartmann layers. *Proc. R. Soc. Lond.* A **300**, 94107.

Roberts, P. H. 1967*b* *An Introduction to Magnetohydrodynamics*. Elsevier.

Shercliff, J. A. 1965 *A Text-book of Magnetohydrodynamics*. Pergamon.